Journal of Nuclear Materials 403 (2010) 147–151

Contents lists available at ScienceDirect

Journal of Nuclear Materials

journal homepage: www.elsevier.com/locate/jnucmat

Electronic ionization induced atom migration in spinel $MgAl_2O_4$

Nan Jiang *, John C.H. Spence

Department of Physics, Arizona State University, Tempe, AZ 85287-1504, United States

ARTICLE INFO

Article history:
Received 22 March 2010
Accepted 7 June 2010

ABSTRACT

We report direct spectroscopic evidence for atom migration during the initial stage of electron irradiation in spinel $MgAl_2O_4$. Time-dependent electron energy-loss spectroscopy of the Mg and Al L_{23} edges shows that both Mg and Al have a tendency to occupy the octahedral interstices under electron irradiation, along with a slight expansion of the Al–O bonding distance, but there is little change in the structural framework of oxygen. The process is irreversible at room temperature.

© 2010 Elsevier B.V. All rights reserved.

1. Introduction

Spinel magnesium aluminate ($MgAl_2O_4$) has potential applications in nuclear energy systems due to its radiation resistance. It retains the spinel structure to a high damage level under fast-neutron or ion-beam irradiation at or above room temperatures [1]. The difficulty in forming voids and dislocation loops may be due to ionization-enhanced recombination of antisite defects [2–4]. Site exchange between Mg on tetrahedral interstices and Al on octahedral interstices has been reported in $MgAl_2O_4$ under neutron irradiation [5]. On the other hand, it was also reported that $MgAl_2O_4$ can undergo a crystalline-to-amorphous transformation through an intermediate crystalline phase by irradiation of Xe^{2+} ions at cryogenic temperatures [6,7]. The intermediate phase was identified to be a "rocksalt-like" structure, in which the oxygen sublattice maintains a "pseudo" cubic close-packed arrangement (as in spinel), while the Mg and Al occupy randomly the octahedral lattice interstices [8]. The disorder on the Al and O sublattices but not on the Mg sublattice after ion irradiation has also been reported [9]. Under energetic electron (1 MeV) bombardment, the $MgAl_2O_4$ underwent a progressive phase transformation (spinel → γ-alumina) along with the gradual decrease of Mg, between 750 and 850 °C, and did not produce any dislocation-related damage [10]. By contrast, dislocation loops were formed by 1 MeV electron irradiation, followed by precipitation of metallic Mg, in the range 900–1130 K [11,12]. It has also been reported that electron irradiation induces cation disorder between the tetrahedral and octahedral sites at 870 K, and slight evacuation of cations from the tetrahedral to octahedral sites also occurs [13]. The conflicting roles of ionizing radiation have also been discussed in some ceramics [14]. The variety of behaviors may be partly due to the variety of irradiation conditions, which involve different radiation sources, energies, stoichiometry, and specimen temperatures.

Fundamentally, the intrinsic radiation resistance of a material does not depend on the sensitivity of the technique used to evaluate the degree of damage. However, some techniques are better suited to monitor the radiation damage degradation processes that are occurring than others. Most previous studies have relied on transmission electron microscopy (TEM) images and electron diffraction to identify dislocation loops, voids, defect clusters and new phases, which are in fact the end-product of the damage processes. Due to the complexity of these processes, such post-radiation observations do not reveal the initial process of radiation damage, and may cause confusion as to the fundamental mechanisms of damage in $MgAl_2O_4$ and other materials. Therefore, *it is critically important to be able to observe the initial stages of atomic migration, which is the origin of all subsequent microstructure and property change*.

Here we combine electron irradiation with time-dependent electron energy-loss spectroscopy (EELS) to directly observe atom migration in $MgAl_2O_4$ during the initial stages of electron irradiation. This method is equivalent to the "pump–probe" technique. The irradiation process is pumped by a beam of electron, and the irradiation effects are simultaneously probed by the same beam of electron, through the electron energy-loss near edge structure (ELNES) in real time. The core edge ELNES is determined by the partial electronic density of states (DOS) projected onto the species that undergo electronic excitation, and thus is very sensitive to the local structure and chemistry [15]. Therefore, it has long been used to identify nearest-neighbor coordination (fingerprints) [16]. The basic idea of this work is as follows. Providing that the Mg and Al migrate between tetrahedral and octahedral interstitial sites under electron irradiation, the ELNES of the Mg and Al core edges should show time-dependent changes, which can be directly related to the initial process of electron irradiation in $MgAl_2O_4$. This is possible using EELS because of the parallel detection capability, which, together with a field emission electron source (with greater brightness than current synchrotrons), provides much higher count rates than are possible using X-ray absorption near edge

* Corresponding author.
E-mail address: nan.jiang@asu.edu (N. Jiang).

0022-3115/$ - see front matter © 2010 Elsevier B.V. All rights reserved.
doi:10.1016/j.jnucmat.2010.06.013

structure (XANES). Unlike photons, electrons are not annihilated in an inelastic interaction, and continue to the detector after an energy-loss event. It is therefore possible to operate every energy-loss detection channel in a magnetic quadrant spectrometer simultaneously. This high detection efficiency allows the time-evolution of spectra to be studied in detail, with the very high spatial resolution of the electron nanoprobe.

2. Experiment and calculation

A prerequisite for this analysis is the proper interpretation of the Mg and Al L_{23} edges in $MgAl_2O_4$. However, previous work on the L_{23} edges in $MgAl_2O_4$ is scarce [17,18], although the O K edge has attracted considerable attention [19–21]. In our work, we used the full multiple scattering method with muffin-tin potentials (encoded in FEFF8 software) [22] to simulate the Mg and Al L_{23} edges in a normal spinel, an inverse spinel, and a modified structure. The so-called "final state" approximation for the absorbing atom is used to account for core–hole effects. Restricted by the dipole selection rule, the L_{23} edge is the projection of unoccupied s and d states. Therefore only the sum of the unoccupied s and d DOS is compared with experimental data. The atomic transition matrix has been ignored in this work [23].

The spinel $MgAl_2O_4$ has space group $Fd\bar{3}m$ [24]. Experimental parameters (lattice parameter a = 0.8083 nm, and oxygen parameter u = 0.236) are used in the calculations. In a normal spinel, Mg occupies the tetrahedral interstices and Al occupies the shrunken octahedral interstices. In an inverse spinel, Mg moves to the Al sites and half of the Al move to Mg sites. In addition, calculations were also carried out for a modified structure, in which oxygen occupies the ideal cubic close-packed position (u = 0.25) and both Mg and Al randomly occupy the octahedral interstices. Therefore, the bonding distances of Mg–O and Al–O in this modified structure are 0.21 nm, which is larger than the distances in both normal and inverse spinel structures, which are about 0.19 nm.

$MgAl_2O_4$ crystals were used in this study (Alfa Aesar, >99.9% purity). The crystal structure was confirmed by X-ray diffraction. No impurities were apparent in the energy dispersive characteristic X-ray spectra. TEM specimens were prepared by grinding the $MgAl_2O_4$ into powders in acetone, and picking them up using a Cu grid covered with a lacy carbon thin film. The specimen was then observed and analysed in a JEOL 2010F scanning transmission electron microscope (STEM), operating at 200 keV and TEM mode. The energy resolution of the electron-energy-loss spectrometer is about 1.0 eV, and the collector aperture is about 100 mrad. The energy stability was monitored by the position of the zero-energy-loss peak. The irradiation process was carried out under the conditions that the electron beam was spread to about ~100 nm in diameter, and the beam current measured on the small observation screen was about ~500 PA/cm^2 at a magnification of 100,000 [25]. The acquisition time for each spectrum was 5 s. The conditions were selected as a compromise between a high signal-to-noise ratio for the spectrum, and the damage rate. All observations were at room temperature.

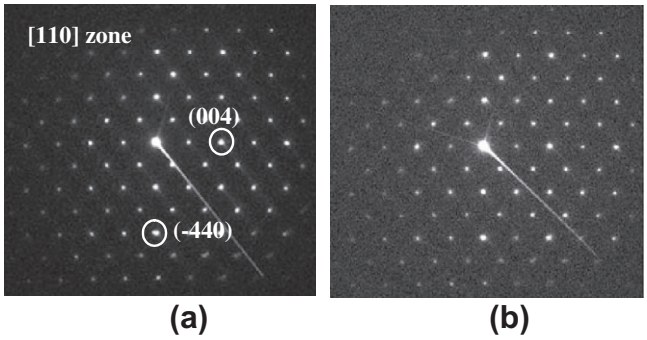

Fig. 1. Time series of selected-area electron diffraction pattern.

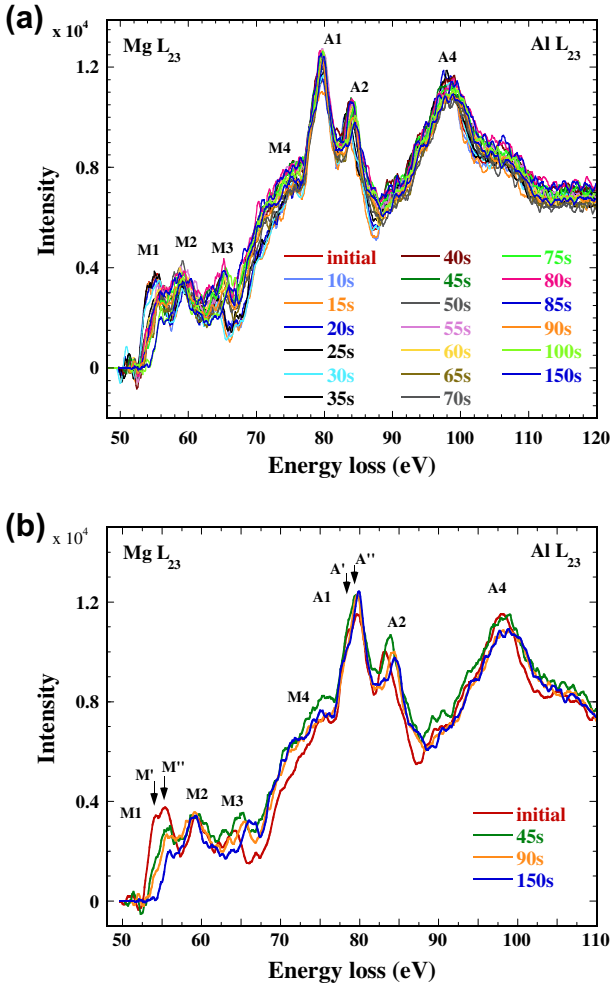

Fig. 2. (a) TREELS of $MgAl_2O_4$ showing progressive changes of Mg and Al L_{23} edges. (b) Comparison of selected spectra from (a).

3. Results and discussion

Fig. 1 shows two kinematical electron diffraction patterns from the same selected area at different time. The sample was tilted to the [1 1 0] direction, and then moved to a nearby "fresh" region to record diffractions. The first (Fig. 1a) was the initial, which is therefore considered to be free from beam damage. A slight deviation from the perfect zone axis is due to the slight difference in orientation between the recording region and the region which was used to tilt the sample. The second (Fig. 1b) was taken in the same selected area after 5 min of irradiation. The exposure time for each diffraction pattern is 0.5 s. Kinematically, there is no difference between Fig. 1a and b: no extra reflections and no extinctions are observed.

Using the similar illumination condition (the same electron beam intensity), we recorded a time-dependent EELS of Mg and Al L_{23} edge in another area, which was away from the low index zone axis to avoid any channeling effect. The result is shown in Fig. 2a. The "initial" spectrum was recorded "immediately" after a "fresh" area was exposed to the electron beam. The time resolu-

tion is determined by the acquisition time of each spectrum, which was 5 s in Fig. 2. For a closer comparison, four selected spectra from the time series are re-plotted in Fig. 2b. Overall, the Mg L_{23} edge (52–76 eV) undergoes dramatic changes, while the Al L_{23} edge (76–110 eV) only has relatively small changes. In the Mg L_{23} edge, four peaks can be recognized in the "initial" spectrum, marked as M1, M2, M3 and M4 respectively. Peak M1 consists of two small sub-peaks (M′ and M″), separated about 1.5 eV. In the high-energy resolution (<0.2 eV) XANES, these two sub-peaks are well separated in a normal spinel $MgAl_2O_4$ [25]. During the irradiation, the intensity of peak M1 (relative to peak M2) drops continuously, and the position of peak M3 shifts gradually towards higher energy. A closer comparison between the "initial" spectrum, and one after 150s of irradiation, shows that the continuous drop of peak M1 results in a threshold shift of about 2.5 eV toward higher energy. It is also noted that the small peak at about 56.0 eV in the spectrum recorded after 150 s of irradiation does not have the same origin as peak M″, which is located at about 55.4 eV. We also noted that peak positions of M2 and M4 are apparently not changed much with the increase of irradiation.

In the Al L_{23} edge (Fig. 2), three peaks, marked A1, A2, and A4, can be recognized. Peak A1 consists of two small peaks, marked A′ and A″. The splitting of sub-peaks A′ and A″ is slightly narrower than that of sub-peaks M′ and M″. This is consistent with XANES results [26]. However, the analysis of the Al L_{23} edge is more difficult than that of the Mg L_{23} edge. First of all, background subtraction is almost impossible, and the progressively changed Mg L_{23} edge makes it even worse. The intensity of sub-peak A′, relative to that of sub-peak A″, drops slightly with increase in irradiation. However, it is difficult to rule out the influence of the Mg L_{23} edge on such a change. Nevertheless, two characteristics of the Al L_{23} edge under electron irradiation are clear. One is that the threshold energy of the Al L_{23} edge does not change, neither does peak position of A1, and the other is that the position of peak A2 moves progressively towards higher energy. In addition, the position of peak A4 does not change.

Obviously the near-edge structures of Mg and Al L_{23} edges are more sensitive to electron irradiation than the kinematical electron diffraction. The changes in the former can be observed nearly immediately after the exposure to electron beam (Fig. 2), while the latter has little observable changes even after 5 min of irradiation (Fig. 1), unless the quantitative measurements were applied. We compared calculations of electron diffraction intensities between a normal spinel structure and the same spinel structure in which all Mg sites are empty. The kinematical results show that the patterns are exactly the same, although the dynamic results show the differences in the relative intensities of some reflections. In other words, atom migration may not always induce extra reflections or cause extinctions. To observe atom migration by diffraction, one must rely on the quantitative measurements, which are also sensitively dependent on thickness and orientation of the sample.

Contrary to the behavior of the Mg and Al L_{23} edges, the bulk plasmon in $MgAl_2O_4$ does not change (Fig. 3). The slight decrease of the plasmon intensity after 150 s of irradiation is probably due to the mass loss induced by electron irradiation. There are two small bumps at about 37.5 and 49.0 eV. The former is probably due to interband transitions, while the later is the plural scattering from the plasmon.

In the insert of Fig. 3, the O K edge recorded in the same area after 150 s of irradiation (Fig. 2) is also compared with one recorded in a nearby "fresh" area. Interestingly, the O K edge does not show any change, even though the Mg and Al L_{23} edges have changed dramatically. This indicates that the structural framework formed by oxygen atoms undergoes little change due to electron irradiation during the period of these observations (Fig. 2).

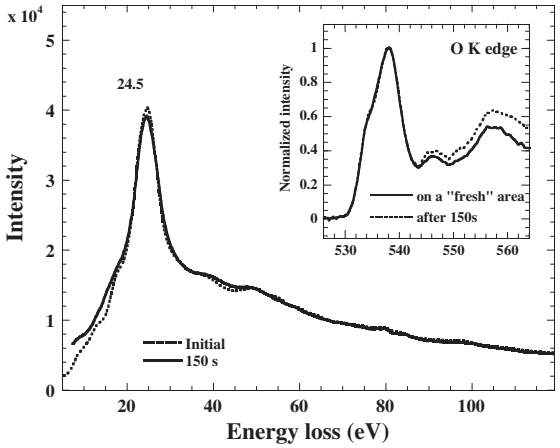

Fig. 3. Comparison of plasmon energy loss (24.5 eV) and O K edge between the initial state and after 150 s of irradiation.

The calculated Mg and Al L_{23} edges (sum of unoccupied s and d DOS) for three different structural models are compared with experimental data in Fig. 4. There is no relative energy shift among the calculations in different models. Overall, the calculation on Mg in the normal spinel fits the "initial" experimental spectrum quite well, although the splitting of the first peak (M1) is not fully reproduced. In both inverse spinel and the modified structures, in which Mg occupies the octahedral interstices, the sharp first peak in the

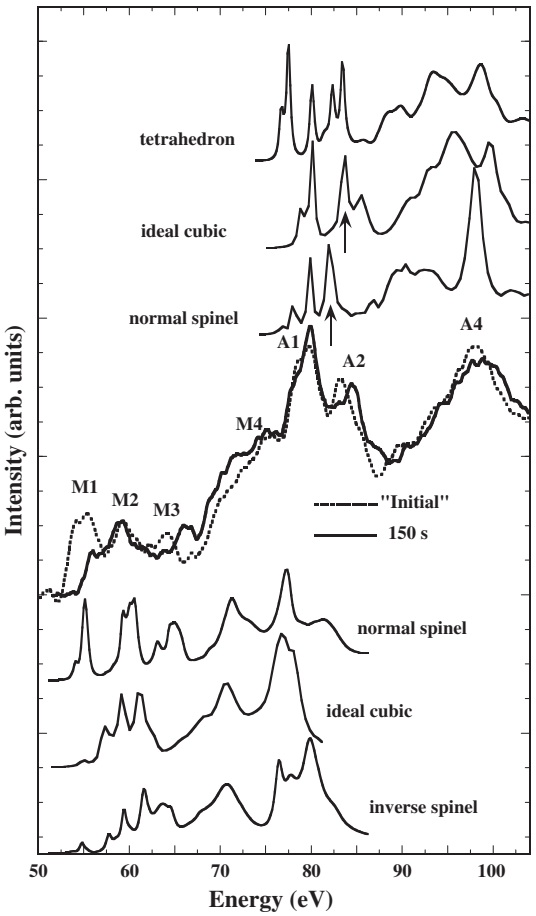

Fig. 4. Comparison of theoretical calculations (thin lines) in three different structures models with experimental data (thick lines). "Ideal cubic" indicates the modified structure, in which oxygen atoms are on the ideal cubic position. "Tetrahedron" refers to the tetrahedral Al in inverse spinel.

normal spinel becomes small bumps, and thus the threshold energies shift towards higher energy. The shift of threshold energy by about 2–3 eV between normal and inverse spinels has also been revealed in ground-state calculations based on density functional theory, within local density approximation (DFT–LDA) [27]. This implies that the progressive shift of the threshold energy of the Mg L_{23} edge observed in the time-dependent EELS is probably induced by the migration of Mg from its original tetrahedral site to the octahedral interstices. However, whether the Al exchanges with Mg, or redistributes within the octahedral interstices cannot be determined from the time-dependent EELS of Mg L_{23} edges. This is because the calculations do not fit the experimental spectrum after 150 s of irradiation in either the inverse spinel or the modified structure, although the later slightly resembles the experiment. One possible reason is that the dynamic structure during electron irradiation is probably much more complicated than the simplified structural models used in these calculations.

The calculation on Al in the normal spinel structure also agrees with the "initial" experimental Al L_{23} edge quite well. All features are reproduced qualitatively, although the position of peak A2 is several eV lower than the experiment and the predicted broad peak between A2 and A4 is not experimentally observed. The relative intensities of peaks are not comparable to the experimental data, since the later is overlapped with the Mg L_{23} edge. In the normal spinel, all Al are on octahedral interstices, while in the inverse spinel, half of Al are on tetrahedral sites. The calculation on tetrahedral Al shows a strong peak prior to the threshold of the Al L_{23} edge in the normal spinel. In the ground-state calculations using DFT–LDA method, the shifted tetrahedral and octahedral Al has also been observed [27]. This implies that the threshold of the Al L_{23} edge would shift towards lower energy if Al moved from octahedral to tetrahedral interstices. However, the threshold shift of the Al L_{23} edge is not observed in the experiment. Therefore, the migration of Mg from tetrahedral to octahedral interstices does not cause the reverse migration of Al from octahedral to tetrahedral interstices.

By comparison with the normal spinel, the calculations in the modified structure clearly show the shift of peak A2 towards higher energy (indicated by arrows in Fig. 4). In both structures, Al are all on the octahedral interstices, but the main difference is that the Al–O bonding distance in the modified structure is longer than in the normal spinel. This indicates that the progressive shift of peak A2 is probably due to the gradual increase of the Al–O bond length.

Therefore, it is reasonable to conclude from the time-dependent EELS observations that under electron irradiation, Mg moves gradually to the octahedral interstices, but Al does not fill back into the tetrahedral interstices, but rather redistributes within the octahedral interstices. In other words, electron irradiation in the spinel $MgAl_2O_4$ has a tendency to create a new "phase" (with both Mg and Al occupying octahedral interstices), but not to cause the normal-to-inverse transition (or cation disorder). We also noted that atom migrations observed by EELS does not induce extra reflections or cause extinctions. This is probably because the O lattice keeps unchanged at the initial stage of damage (Fig. 3). It is also noted that the original spinel cannot be restored in the irradiated area by turning off the electron beam at room temperature. However, the recovery might occur at high temperature. This could be confirmed by using a heating stage in the electron microscope.

The migration of Mg into octahedral interstices as a result of electron irradiation can be qualitatively explained by the following hypothesis. Electronic excitation by fast electrons causes some electrons in atoms to be driven out of the trajectory of the beam. The trajectory region thus becomes positively charged, providing charge neutrality cannot be immediately restored from the surroundings (as in a metal where fast screening occurs) [28–30]. Due to the difference in formal valence states, an Mg on an Al site in an octahedron bears a negative charge $[Mg^{2+}(Al^{3+})]^-$, while an Al on an Mg site in tetrahedron bears a positive charge $[Al^{3+}(Mg^{2+})]^+$ [31–33]. Under a positive electrostatic field, $[Mg^{2+}(Al^{3+})]^-$ becomes more stable, while $[Al^{3+}(Mg^{2+})]^+$ becomes unstable. As a result, both Mg and Al have a tendency to occupy octahedral interstices. There are two implications of this hypothesis. One is that the degree of inversion of $MgAl_2O_4$ spinel should have little effect on the result of atom migration. Both Mg and Al should all occupy the octahedral interstices eventually. Another is that Mg should have a higher mobility in spinel than Al. This is consistent with experiments in which a layer of MgO was precipitated at the cathode when $MgAl_2O_4$ or $MgFe_2O_4$ was placed in an electric field at elevated temperature [34,35]. We also noticed that our observations are opposite to the previous report, in which the intense ionization within individual ion tracks causes disordering of octahedral cations (transfer of octahedral ions to tetrahedral sites) [36].

As we knew, the phenomenon of ionization enhanced and induced atom migration or diffusion has been observed in ceramics previously [37–40], another type of mechanism, knock-on damage, may also play a certain role in the high-energy particle irradiation. In our previous similar study in zircon [41], the knock-on collisions induced preferential sputtering of O from surfaces are responsible for the beam damage on zircon in TEM. In the $MgAl_2O_4$ however, the change in Mg does not accompany the loss of Mg. Therefore, the surface sputtering can be ignored. The knock-on damage inside the specimen requires the threshold displacement energies. According to the equation derived from the law of momentum conservation [41], the maximum atom recoil energy obtained by Mg from 200 keV incident electron is about 32 eV, which is considered smaller than the threshold displacement energy for Mg in $MgAl_2O_4$ [42,43]. Therefore, we can ignore the knock-on damage in this case.

In an electron microscope, most of the electron energy dissipated in energy losses is converted into heat, which can be quickly carried away through thermal diffusion. Under normal illumination conditions in electron microscope, the rises of temperature caused by electron irradiation, which are calculated using the macroscopic equation of heat conduction, are usually several or several tens of degrees only, providing that the specimen has regularly simple geometry and good thermal contact with surroundings [44,45]. However, the local melting of small particles in some cases, which are in poor contact with matrix, have also been observed and attributed to the temperature rise caused by electron irradiation [46–48]. Usually, the thermal equilibrium can be reached very quickly [44]; and the equilibrium time is much shorter than the acquisition time of spectrum in this work. According to equation (10.12) in [44], the temperature rise largely depends on the current rather then the current density. On the contrary, the rates of atom migration and thus the damage rate is highly current density dependent in the $MgAl_2O_4$. At very high current density, atom diffusion become so rapidly that O_2 may even form in the irradiated region [49]. Therefore, we believe that the effect of temperature rise by electron irradiation can be ignored, in comparison with the electronic excitations.

4. Conclusion

In conclusion, we find that $MgAl_2O_4$ is susceptible to electron irradiation. Using time-dependent EELS, site-specific atom migration during the initial stage of irradiation can be observed. Under electron irradiation, we find that all cations (both Mg and Al) have a tendency to occupy the octahedral interstices.

Acknowledgments

This work is supported by NSF DMR0603993. The use of facilities within the Center for Solid State Science at ASU is also acknowledged.

References

[1] F.W. Clinard, G.F. Hurley, L.W. Hobbs, J. Nucl. Mater. 108 (9) (1982) 655.
[2] L.W. Hobbs, F.W. Clinard Jr., J. Phys. 41 (C6) (1980) 232.
[3] C. Kinoshita, K. Fukumoto, K. Fukuda, F.A. Garner, G.W. Hollenberg, J. Nucl. Mater. 219 (1995) 143.
[4] S.J. Zinkle, Nucl. Instrum. Methods B 91 (1994) 234.
[5] K.E. Sickafus et al., J. Nucl. Mater. 219 (1995) 128.
[6] R. Davanathan, K.E. Sickafus, N. Yu, M. Nastasi, Philos. Mag. Lett. 72 (1995) 155.
[7] K.E. Sickafus, N. Yu, M. Nastasi, J. Nucl. Mater. 304 (2002) 237.
[8] M. Ishimaru, I.V. Afanasyev-Charkin, K.E. Sickafus, Appl. Phys. Lett. 76 (2000) 2556.
[9] A. Turos, H. Matzke, A. Drigo, A. Sambo, R. Falcone, Nucl. Instrum. Methods Phys. Res. B 113 (1996) 261.
[10] S.J. Shaibani, S.N. Buckley, M.L. Jenkins, Radiat. Effects 99 (1986) 485.
[11] S.N. Buckley, Fusion technology, in: Proc. of the 13th Symposium, vol. 2, Vasere, Italy, 1984, p. 1011.
[12] K. Yasuda, C. Kinoshita, R. Morisaki, H. Abe, Philos. Mag. A 78 (1998) 583.
[13] T. Soeda, S. Matsumura, C. Kinoshita, N.J. Zaluzec, J. Nucl. Mater. 283–287 (2000) 952.
[14] S.J. Zinkle, V.A. Skuratov, D.T. Hoelzer, Nucl. Instrtrum. Methods B 191 (2002) 758.
[15] J. Fink, in: J.C. Fuggle, J.E. Inglesfield (Eds.), Unoccupied Electronic States, Springer-Verlag, Berlin, 1992, pp. 203–239.
[16] R.F. Egerton, Electron Energy-loss Spectroscopy in the Electron Microscopy, second ed., Plenum Press, New York, 1996. pp. 363–369 (and references therein).
[17] J. Bruley, M. Tseng, D.B. Williams, Microsc. Microanal. Microstruct. 6 (1995) 1.
[18] S. Mo, W.Y. Ching, Phys. Rev. B 62 (2000) 7901.
[19] S. Köstlmeier, C. Elsässer, Phys. Rev. B 60 (1999) 14025.
[20] D.W. McComb, A.J. Craven, L. Chioncel, A.I. Lichtenstein, F.T. Docherty, Phys. Rev. B 68 (2003) 224420.
[21] K. van Benthem, H. Kohl, Micron 31 (2000) 347.
[22] A.L. Ankudinov, B. Ravel, J.J. Rehr, S. Conradson, Phys. Rev. B 58 (1998) 7565.
[23] R.D. Leapman, P. Rez, D.F. Mayers, J. Chem. Phys. 72 (1980) 1232.
[24] R.W.G. Wyckoff, Crystal Structures, second ed., Wiley, New York, 1965. p. 75.
[25] This is equivalent to electron flux rate of 8.0×10^5 e/nm^2·s on the sample.
[26] W.L. O'Brien et al., Phys. Rev. B 47 (1993) 15482.
[27] S. Mo, W.Y. Ching, Phys. Rev. B 54 (1996) 16555.
[28] J. Cazaux, Ultramicroscopy 60 (1995) 411.
[29] N. Jiang, J. Qiu, A.L. Gaeta, J. Silcox, Appl. Phys. Lett. 80 (2002) 2005.
[30] A. Howie, Microsc. Microanal. 10 (2004) 685.
[31] G.S. White, R.V. Jones, J.H. Crawford Jr., J. Appl. Phys. 53 (1981) 265.
[32] L.S. Cain, G.J. Pogatshnik, Y. Chen, Phys. Rev. B 37 (1988) 2645.
[33] V.T. Gritsyna, I.V. Afanasyev-Charkin, V.A. Kobyakov, K.E. Sickafus, J. Am. Ceram. Soc. 82 (1999) 3365.
[34] J.R. Martinelli, E. Sonder, R.A. Weeks, R.A. Zuhr, Phys. Rev. B 33 (1986) 5698.
[35] M.T. Johnson, C.B. Carter, H. Schmalzried, J. Am. Ceram. Soc. 83 (2000) 1768.
[36] S.J. Zinkle, Hj. Matzke, V.A. Skuratov, Microstructure of swift heavy ion irradiated $MgAl_2O_4$ spinel, in: S.J. Zinkle, G.E. Lucas, R.C. Ewing, et al. (Eds.), Microstructural Processes During Irradiation, vol. 540, Materials Research Society, Warrendale, PA, 1999, pp. 299–304.
[37] J.C. Bourgoin, J.W. Corbett, J. Chem. Phys. 59 (1973) 4042.
[38] J.C. Bourgoin, J.W. Corbett, Radiat. Effects 36 (1978) 157.
[39] A.I. Ryazanov, K. Yasuda, C. Kinoshita, A.V. Klaptsov, J. Nucl. Mater. 323 (2003) 372.
[40] S.J. Zinkle, J. Nucl. Mater. 219 (1995) 113.
[41] N. Jiang, J.C.H. Spence, J. Appl. Phys. 105 (2009) 123517.
[42] R. Smith, D. Bacorisen, B.P. Uberuaga, K.E. Sickafus, J.A. Ball, R.W. Grimes, J. Phys.: Condens. Matter 17 (2005) 875.
[43] S.J. Zinkle, C. Kinoshita, J. Nucl. Mater. 251 (1997) 200.
[44] L. Reimer, Transmission Electron Microscopy, Springer Series in Optical Sciences, vol. 36, Springer-Verlag, Berlin, 1989. pp. 431–439.
[45] H. Kohl, H. Rose, H. Schnabl, Optik 58 (1984) 11.
[46] T. Yokota, M. Murayama, J.M. Howe, Phys. Rev. Lett. 91 (2003) 265504.
[47] S.A. Nepijko, M. Klimenkov, H. Kuhlenbeck, H.-J. Freund, Cryst. Res. Technol. 35 (2000) 745.
[48] V.G. Gryaznov, A.M. Kaprelov, Yu. Belov, Philos. Mag. Lett. 63 (1991) 275.
[49] N. Jiang, J.C.H. Spence, Ultramicroscopy 106 (2006) 215.